Engineering 6 (2020) 68–76

Contents lists available at ScienceDirect

Engineering

journal homepage: www.elsevier.com/locate/eng

Research
Intelligent Manufacturing—Article

Development of an *In-Situ* Laser Machining System Using a Three-Dimensional Galvanometer Scanner

Xiao Li [a,b], Bin Liu [a,b,*], Xuesong Mei [a,b], Wenjun Wang [a,b], Xiaodong Wang [a,b], Xun Li [c]

[a] State Key Laboratory for Manufacturing Systems Engineering, Xi'an Jiaotong University, Xi'an 710049, China
[b] Shaanxi Key Laboratory of Intelligent Robots, Xi'an Jiaotong University, Xi'an 710049, China
[c] Xi'an Institute of Optics and Precision Mechanics, Chinese Academy of Sciences, Xi'an 710119, China

ARTICLE INFO

Article history:
Received 4 April 2019
Revised 14 June 2019
Accepted 12 July 2019
Available online 21 November 2019

Keywords:
In-situ laser machining
Three-dimensional galvanometer scanner
Line structured light
Three-dimensional measurement

ABSTRACT

In this study, a three-dimensional (3D) *in-situ* laser machining system integrating laser measurement and machining was built using a 3D galvanometer scanner equipped with a side-axis industrial camera. A line structured light measurement model based on a galvanometer scanner was proposed to obtain the 3D information of the workpiece. A height calibration method was proposed to further ensure measurement accuracy, so as to achieve accurate laser focusing. *In-situ* machining software was developed to realize time-saving and labor-saving 3D laser processing. The feasibility and practicability of this *in-situ* laser machining system were verified using specific cases. In comparison with the conventional line structured light measurement method, the proposed methods do not require light plane calibration, and do not need additional motion axes for 3D reconstruction; thus they provide technical and cost advantages. The *in-situ* laser machining system realizes a simple operation process by integrating measurement and machining, which greatly reduces labor and time costs.

© 2020 THE AUTHORS. Published by Elsevier LTD on behalf of Chinese Academy of Engineering and Higher Education Press Limited Company. This is an open access article under the CC BY-NC-ND license (http://creativecommons.org/licenses/by-nc-nd/4.0/).

1. Introduction

Over the past 20 years, laser machining technology has found its way into many industrial applications, such as welding [1–3], cutting [4,5], drilling [6,7], texturing [8–10], and micro-structures manufacturing [11–13]. With the development of laser machining technology and equipment, the application of this technology has gradually become popularized, from mass production to small batch customized production. It is essential to develop a laser machining technique that is more suitable for diversified products, and the advent of the galvanometer scanner greatly assists in this endeavor. A galvanometer scanner can quickly and accurately control the position of the laser spot. Compared with traditional processing methods, laser processing with a galvanometer scanner has many advantages, including high dynamic performance and processing speed, no wear on mechanical tools, contact-free processing, and exceptional flexibility without retooling [14–16].

The major challenge of three-dimensional (3D) laser machining is to continually keep the laser focus spot on a specific position in 3D space [17,18]. Noh et al. [19] proved that the microgrooves produced by an on-focus laser possess higher quality in terms of depth and uniformity compared with those produced by an off-focus laser. Cao et al. [17,20] used machine vision to compensate for a defocused laser and to continually keep the laser focused on the surface. Wang et al. [21] divided a large freeform surface into sub-areas, sub-layers, and sub-blocks to ensure that the laser was always focused. Based on the 3D surface of the workpiece, dynamic adjustment of the laser focus spot in the spatial position is the key to realizing non-planar laser machining. The 3D galvanometer scanner improves the laser beam by allowing it to change its focus position rapidly in 3D space; the 3D machining capability of the galvanometer scanner benefits from its dynamic focusing unit [22,23]. Xiao et al. [24] used a 3D galvanometer scanner to directly mark patterns on freeform curved surfaces. Diaci et al. [25] used a 3D galvanometer scanner to mark complete patterns on a curved surface and inclined surface, which could not be done using a general 2D galvanometer scanner.

Most current 3D galvanometer scanner machining systems are unable to perform 3D measurement; therefore, it is necessary to obtain the 3D information of the workpiece by means of 3D software modeling or special scanning equipment before laser

* Corresponding author.
E-mail address: liubin1110@xjtu.edu.cn (B. Liu).

https://doi.org/10.1016/j.eng.2019.07.024
2095-8099/© 2020 THE AUTHORS. Published by Elsevier LTD on behalf of Chinese Academy of Engineering and Higher Education Press Limited Company.
This is an open access article under the CC BY-NC-ND license (http://creativecommons.org/licenses/by-nc-nd/4.0/).

machining, and the workpiece must be positioned by fixtures. However, when workpieces are produced in a small batch and are diversified, a great deal of time will be spent on preparation work, resulting in increased hardware and time costs. At the same time, multiple processes may introduce more errors. *In-situ* processing technology generally refers to direct *in-situ* measurement and processing on an object; this technology has been investigated in the fields of industry, bioengineering, and more [26–29]. When this technology is used in 3D laser machining, its main advantage lies in the integration of measurement and machining, which can simplify the traditional workflow—including individual modeling, clamping, adjustment, and alignment—and avoid the workload and errors caused by redundant processes. The galvanometer scanner can project line structured light for 3D measurement [30–32]. Diaci et al. [25] attempted to use a laser system for measurement and machining in order to complete rapid and flexible laser marking and engraving; however, they did not provide a specific implementation method for measurement or a detailed evaluation of the results.

Traditional 3D measurement using line structured light is mainly based on the direct projection of laser lines onto the surface of an object [33]. Zhou et al. [34] used line structured light to measure rails; they found that the errors in length, width, and thickness were about 0.3 mm. Liu et al. [35] measured the diameter of an axis (the diameter was about 30 mm) by means of line structured light. The diameter was obtained by fitting the measured points, and the error was found to be less than 20 μm. Li et al. [36] used line structured light to measure a cube with a height of 100 mm, and observed an error of about 1 mm. In fact, the absolute measurement accuracy is determined by factors such as the equipment, measurement distance, and algorithm. For example, a small camera field of view and a short measurement distance can result in relatively high measurement accuracy.

The current research on line structured light measurement method mainly includes measurement modeling, the optical center extraction method, and the calibration method. Measurement modeling is the basis of this technology, and is mainly based on geometric derivation. The measurement modeling using a galvanometer scanner is different from the typical method due to the use of the galvanometer scanner and different types of focusing lens. Optical center extraction is an important factor in measurement accuracy. The optical center extraction method with subpixel precision can achieve relatively high measurement accuracy, and there are mainly three types of typical subpixel methods including the Gaussian fitting method [37], gray centroid method [5], and Hessian matrix method [38]. Calibration mainly involves camera parameters calibration and light plane equation calibration. The calibration of the light plane equation is more difficult, and the problem of how to obtain high-precision control points to fit the light plane is a key issue in calibration.

In this study, a 3D *in-situ* laser machining system integrating laser measurement and machining was built using a 3D galvanometer scanner and an industrial camera. The main contribution of this paper is the realization of the integration of *in-situ* measurement and machining, including: ① the proposal of a line structured light measurement model based on a galvanometer scanner; ② the proposal of a height calibration method to ensure measurement accuracy; and ③ the development of *in-situ* machining software to realize time-saving and labor-saving 3D laser processing. The feasibility and practicability of this *in-situ* laser machining system were verified through specific cases. In comparison with the conventional line structured light measurement method, the proposed methods do not require light plane calibration, and do not require additional motion axes for 3D reconstruction. The proposed *in-situ* laser machining system realizes a simple operation process, which reduces labor and time costs.

2. Methods

2.1. 3D measurement method

Fig. 1(a) shows the 3D measurement model based on the line structured light projected by the galvanometer scanner. There are four coordinate systems in this model: the world coordinate system O_w–$x_w y_w z_w$, the galvanometer coordinate system O_g–$x_g y_g z_g$, the camera coordinate system O_c–$x_c y_c z_c$, and the image coordinate system O–uv. To simplify the model, the galvanometer coordinate system is coincident with the world coordinate system. In this research, a non-telecentric f–θ field lens was used. In Fig. 1(a), point a is the center of the galvanometer scanner's y-axis mirror,

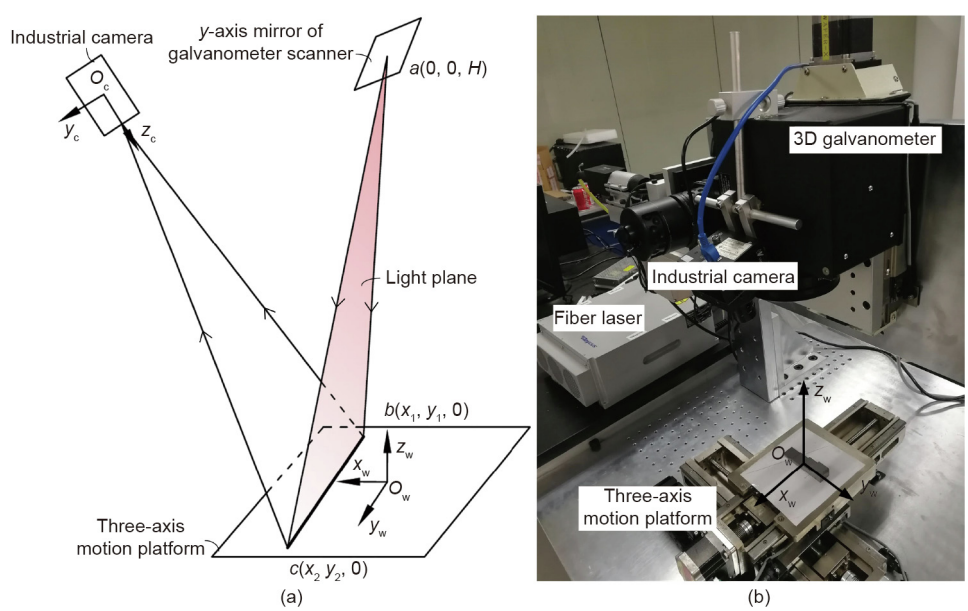

Fig. 1. Principle and equipment diagram of the 3D measurement subsystem. (a) Schematic diagram of the measurement method based on line structured light using the galvanometer scanner; (b) equipment diagram of the measurement and machining system.

whose world coordinates are $a(0, 0, H)$, where H is the height of point a in the world coordinates. Points b and c are the two endpoints of the laser line projected by the galvanometer scanner. Their world coordinates can be precisely controlled by the galvanometer scanner, and are $b(x_1, y_1, 0)$ and $c(x_2, y_2, 0)$. To obtain the 3D coordinates of a point on the object, at least three constraints should be known. According to the typical pinhole camera model [39], Eq. (1) can be derived.

$$\begin{cases} u = f_x \dfrac{x_c}{z_c} + c_x \\ v = f_y \dfrac{y_c}{z_c} + c_y \end{cases} \tag{1}$$

where f_x and f_y are the focal distance expressed in units of horizontal and vertical pixels; and c_x and c_y are the principal point coordinates. Suppose that a space point d, (x_c, y_c, z_c) has the coordinates of d in the camera coordinate system, and (u, v) are the coordinates in the pixel coordinate system. In order to uniquely determine the coordinate value of the point, at least one more constraint is required—that is, the light plane equation. The conventional line structured light measurement method requires calibration of the light plane to determine the light plane equation, but the light plane generated by the galvanometer scanner can be precisely controlled. The laser is focused by the field lens, which includes the non-telecentric f–θ field lens and the telecentric f–θ field lens. When using a non-telecentric f–θ field lens, the light plane in the world coordinate system passes through the three points a, b, and c (Fig. 1(a)); when using a telecentric f–θ field lens, the light plane is always perpendicular to the xy plane in the world coordinate system, and the world coordinates of the point a in Fig. 1 are considered to be $a(x_1, 0, H)$. Therefore, the three known non-collinear points (a, b, and c) in the world coordinate system can be converted to the camera coordinate system according to the camera's external parameters, and the light plane equation in the camera coordinate system can be determined as follows:

$$A \cdot x_c + B \cdot y_c + C \cdot z_c + D = 0 \tag{2}$$

where A, B, C, and D are the coefficients of the light plane equation. This is synchronized with Eq. (1) to obtain Eq. (3):

$$\begin{bmatrix} f_x & 0 & c_x - u \\ 0 & f_y & c_y - v \\ A & B & C \end{bmatrix} \begin{bmatrix} x_c \\ y_c \\ z_c \end{bmatrix} = \begin{bmatrix} 0 \\ 0 \\ -D \end{bmatrix} \tag{3}$$

Thus, coordinates on the pixel coordinate system (u, v) can be converted to the camera coordinate system (x_c, y_c, z_c) according to Eq. (3), and then to the world coordinate system (x_w, y_w, z_w) according to Eq. (4), where $\boldsymbol{R}$ is the rotation matrix and $\boldsymbol{T}$ is the translation matrix in the camera's external parameters.

$$\begin{bmatrix} x_w \\ y_w \\ z_w \end{bmatrix} = \boldsymbol{R}^{-1} \left(\begin{bmatrix} x_c \\ y_c \\ z_c \end{bmatrix} - \boldsymbol{T} \right) \tag{4}$$

2.2. Height calibration method

On the basis of the methods described above, this study introduces the use of a height calibration method to ensure the measurement accuracy of the height direction. The principle of this method is to find the relationship among the actual height, the laser line offset distance, and the pixel distance; this relationship is shown in Eq. (5).

$$Z = f(x, p) \tag{5}$$

where Z is the actual height, x is the laser line offset distance, p is the pixel distance, and f represents the function of x and p. In this study, the laser line is parallel to the y-axis direction in the world coordinate system, and its offset direction is along the x-axis direction, as shown in Fig. 1(a). The three-axis motion platform can be controlled to move a certain distance in the z-axis direction and simultaneously take multiple laser line images for height calibration.

The center coordinate of the laser line in the pixel coordinate system is the optical center. The optical center with a height of 0 and a laser line offset distance of 0 is defined as the reference optical center, and the average pixel distance between any other optical center and the reference optical center is defined as P. In the plane with a height of 0, the average pixel distance between other optical centers and the reference optical center is defined as P_1. When the laser line offset distance is the same and the height is different, the average pixel distance between optical centers at different heights and the optical center at a height of 0 is defined as P_2. Therefore, Eq. (6) is obtained in the pixel coordinate system.

$$P = P_1 + P_2 \tag{6}$$

Fig. 2(a) shows the relationship between P_1 and x (−30 to 30 mm, calibrated every 5 mm). Fig. 2(b) shows the relationship between P_2 and Z (−15 to 15 mm, calibrated every 5 mm). It can be seen from the figures that P_1 has a good linear relationship with x, and P_2 has a good linear relationship with Z.

Fig. 3 plots the relationship among Z, P_2, and x, which is almost fitted to a plane. Therefore, when calculating the actual height Z, P_1 is first calculated by linear interpolation according to the value of x in Fig. 2(a); next, according to the calculated value of P, P_2 can be obtained using Eq. (6). Finally, Z is obtained by interpolation using P_2 and x, as shown in Fig. 3.

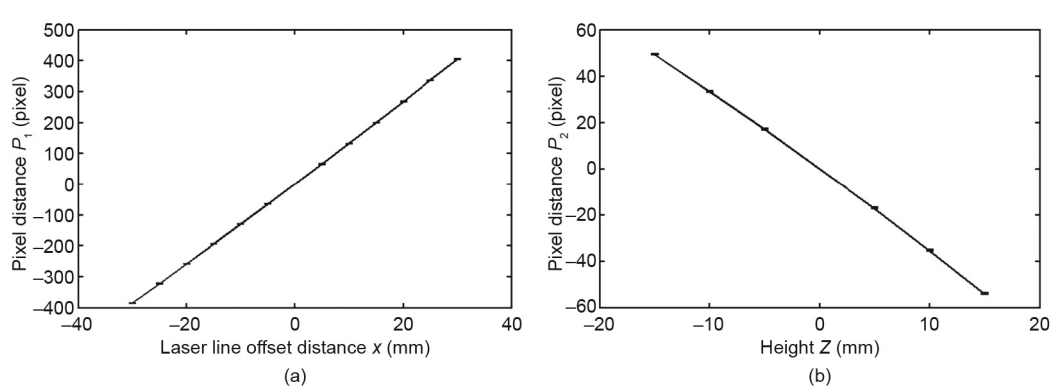

Fig. 2. (a) Relationship between the average pixel distance P_1 and the laser line offset distance x in the height of 0; (b) relationship between the average pixel distance P_2 and the height Z in the laser line offset distance of 0.

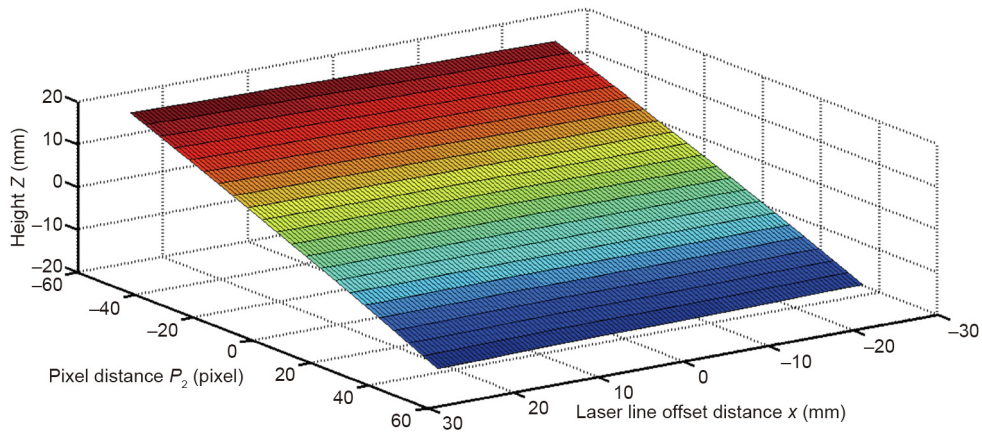

Fig. 3. 3D map of the relationship among the actual height Z, pixel distance P_2, and laser line offset distance x.

2.3. Optical center extraction method

In this method, the laser line images are preprocessed by median filtering, and the gray centroid method is then used to extract the optical center. First, the point $g_{\max}$ with the highest light intensity in a column of pixels is found, and then a gray threshold $K = k \times g_{\max} (0 < k < 1)$ is determined. Here, k is a scale factor, and the pixel coordinates of all points whose gray value is larger than K are set to u_i $(i = 0, 1, 2 \cdots)$; and the corresponding gray values of these points are set to g_i $(i = 0, 1, 2 \cdots)$. Finally, the optical center U is obtained by Eq. (7):

$$U = \frac{\sum_{i=1}^{n} g_i \times u_i}{\sum_{i=1}^{n} g_i} \tag{7}$$

During the extraction of the optical center by the gray centroid method, the thresholds of each column of pixels are different, so even if the gray distribution is not uniform, it will not bring great errors to the determination of the optical center position, thus improving the extraction accuracy.

2.4. In-situ *machining method*

After the extraction of the optical center, the 3D point cloud surface of the object can be obtained according to the methods described in Sections 2.1 and 2.2. The density of the point cloud is determined by the distance between the projected laser lines and the resolution of the industrial camera. The point cloud surface can reflect the actual 3D shape and pose of the object.

After obtaining the surface point cloud of the object, machining patterns or paths are projected to the corresponding position on the point cloud to generate the 3D galvanometer scanner processing instructions. In this study, the machining patterns were projected onto the 3D point cloud in the form of pixels. Each pixel in the machining pattern could find its adjacent points in the point cloud, and the average height value of these points was taken as the height value of the pixel. In order to realize *in-situ* machining, *in-situ* machining software was developed, which achieves the precise projection of patterns at any position of the workpiece by zooming, translating, and rotating the imported patterns.

3. Experiments and evaluation

3.1. Equipment condition

The 3D galvanometer scanner used in this study was a SCANLAB intelliSCAN$_{se}$ 14 equipped with a 255 mm focal length non-telecentric f–θ field lens. The industrial camera was a Vieworks VH-5MG 5-million-pixel black-and-white camera, equipped with a U-TRON FV1520 lens, and the camera was fixed on the side of the 3D galvanometer scanner. The field of view of the industrial camera was about 200 mm × 200 mm when the working distance was 350 mm. The laser source was a 1064 ns fiber laser (RFL-P30Q) with a 680 nm indicator light. The 3D galvanometer scanner was mounted on a three-axis motion platform, as shown in Fig. 1(b).

3.2. 3D measurement accuracy evaluation

The measurement accuracy directly decides the laser focusing accuracy during *in-situ* processing. A standard-height step block was selected (Fig. 4(a)) with a length of 80 mm, a width of 20 mm, and four standard heights of 3, 5, 10, and 15 mm for the measurement accuracy test. The scanned laser line spacing was 0.5 mm, the scanning speed of the galvanometer scanner was 5000 mm·s^{-1}, and the exposure time of the industrial camera was 50 ms. 3D point clouds were generated using Method 1 (the method using the camera parameters and the light plane equation) and Method 2 (the method that includes height calibration). Fig. 4(b) shows the point cloud obtained by Method 2, which accurately reconstructs the height information of the standard-height step block. Fig. 5(a) indicates the average value of the measured height. Fig. 5(b) shows that the error of Method 1 varies with change in the y value. The error at both ends is large, and reaches a maximum at a height of 15 mm, where it exceeds 1 mm. In contrast, the error of Method 2 is stable in the height direction. It is always within the range of ±0.2 mm, and does not change significantly with change in the y value.

The y value of the first and last points of the laser lines scanned onto the workpiece were extracted, and the length of the workpiece obtained by the scanning was calculated to be (79.900 ± 0.154) mm, which is consistent with the actual workpiece length of 80 mm.

3.3. Implementation and examples

3.3.1. Case 1: In-situ *machining on a standard-height step block*

In order to verify the function of the 3D *in-situ* laser machining system developed in this study, 3D measurement, pattern projection, and *in-situ* machining were carried out on a standard-height step block (Fig. 4(a)). This process included the following steps:

Step 1: Pre-calibration work. The Matlab camera calibration toolbox was used to perform camera calibration in order to obtain the camera's internal and external parameters. When obtaining the external parameters, the x-axis and y-axis direction lines were

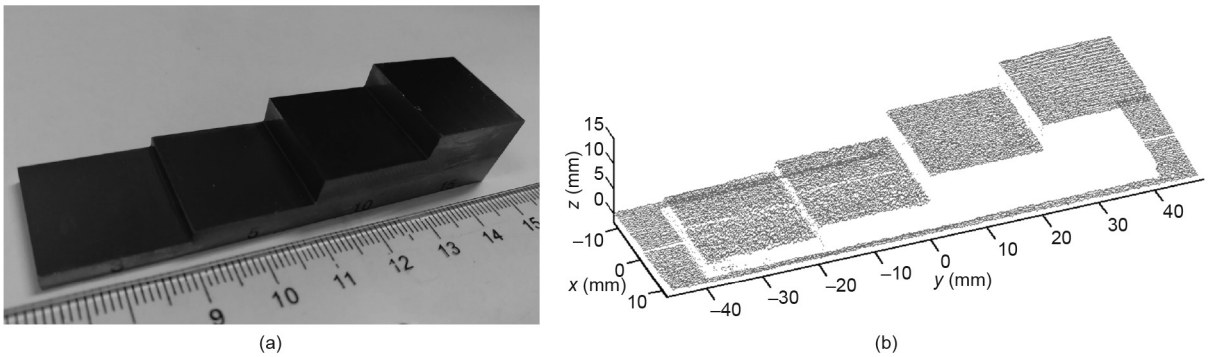

Fig. 4. (a) The standard-height step block with standard heights of 3, 5, 10, and 15 mm; (b) 3D point cloud of the standard-height step block obtained by Method 2.

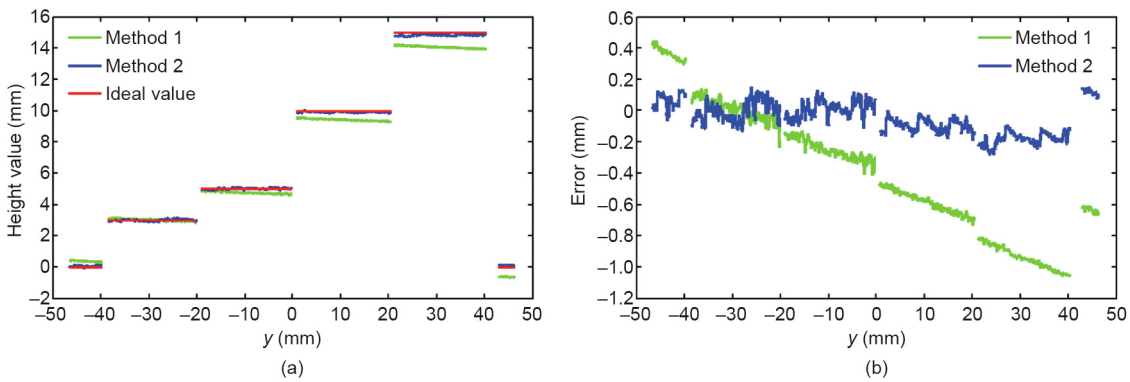

Fig. 5. (a) Average height values obtained by Method 1 and Method 2; (b) height error of Method 1 and Method 2.

projected to the chessboard to coincide the galvanometer coordinate system with the world coordinate system, as shown in Fig. 6(a). Height calibration was performed using the method described in Section 2.2.

Step 2: 3D *in-situ* measurement. The scanning speed of the galvanometer scanner was 5000 mm·s^{-1}, the exposure time of the camera was 50 ms, and the laser line was scanned every 0.5 mm to traverse the object. One of the laser line images is shown in Fig. 6(b). The optical center extracted by the gray center method is illustrated in Fig. 6(c). The 3D point cloud of the workpiece surface was generated according to the methods described in Sections 2.1 and 2.2.

Step 3: Machining pattern projection. The generated 3D point cloud and the imported machining patterns were displayed by OpenGL. After a certain amount of zooming, translating, and rotating, the pattern was projected and displayed on the point cloud.

Step 4: 3D *in-situ* machining. In order to protect the standard-height step block, thermal paper was attached to it, and the laser was used to mark the patterns on the thermal paper. After *in-situ* machining, these patterns were consistent with the design patterns, as shown in Fig. 6(d).

In this study, the *in-situ* machining software (Fig. 7) was developed on a C# WinForm platform. The main functions of the software include scanning laser lines, importing the point cloud, importing machining patterns, translating and rotating the patterns, generating projection patterns, and controlling the galvanometer scanner and the three-axis motion platform.

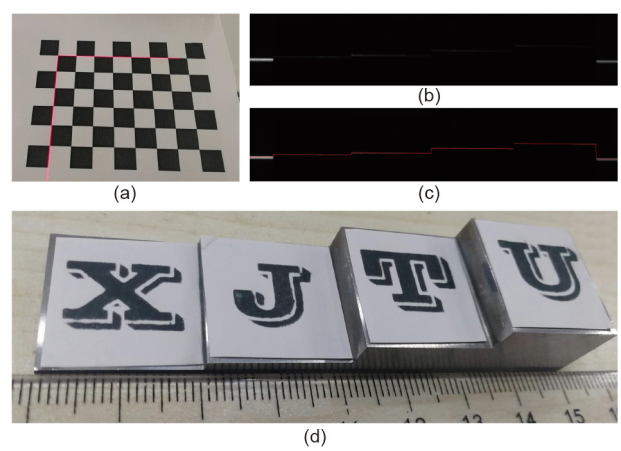

Fig. 6. Implementation process and results of Case 1. (a) The galvanometer coordinate system is coincided with the world coordinate system during camera calibration; (b) one of the laser line images during 3D measurement; (c) the optical center extracted from the laser line image, where the red line is the extracted optical center; (d) *in-situ* machining results on the thermal paper.

3.3.2. Case 2: Local scanning and in-situ machining

When the workpiece is large, it is only necessary to scan the local part that needs to be processed in order to further reduce the unnecessary workload. In this case, a larger non-standard workpiece was selected, as shown in Fig. 8(a), the machining results were shown in Fig. 8(b). It is only necessary to ensure that the local part to be processed is within the processing range of the galvanometer scanner and the visual field of the camera. Figs. 8(c) and (d) show the measurement results of a local corner of the workpiece. Two quick response (QR) code patterns were projected on it, and the machining was directly processed after the projection. Designed patterns can be accurately marked at the corresponding position of the workpiece, which is very convenient. From the machining results, it can be seen that the processed

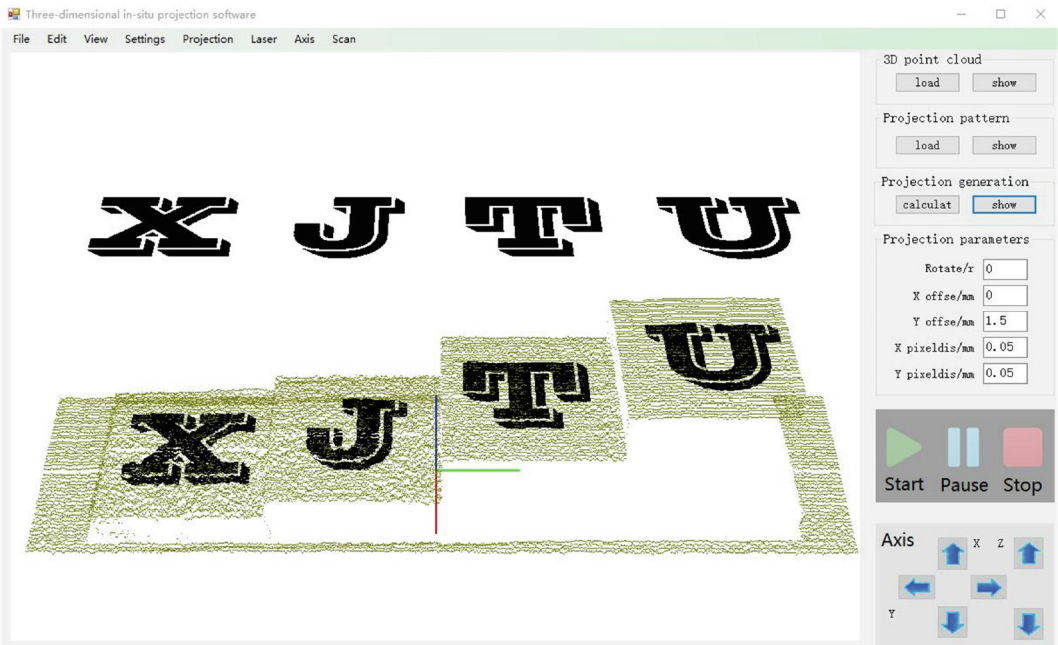

Fig. 7. The *in-situ* 3D machining software interface displays the 3D point cloud (brown dots) of the standard-height step block and of the machining patterns before and after projection.

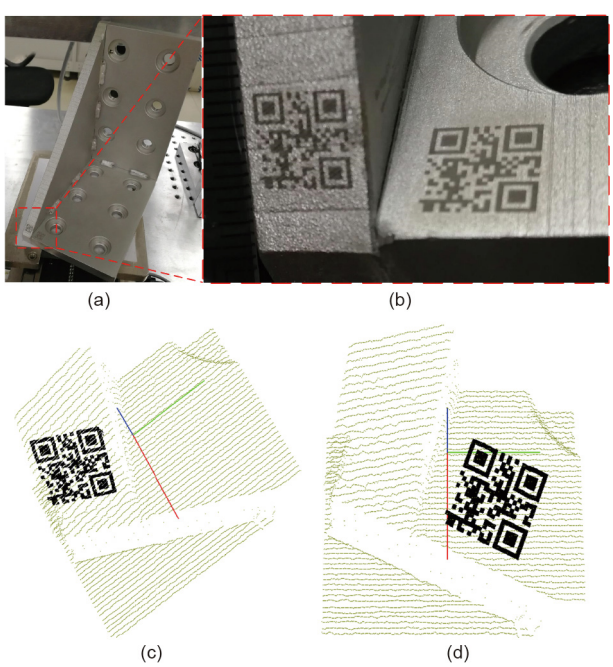

Fig. 8. Implementation process and results of Case 2. (a) A larger size non-standard workpiece on the machining platform; (b) *in-situ* machining results of two QR code patterns at the corner of the workpiece; (c) projection results on the slope; (d) projection results on the plane.

patterns are complete and have no obvious flaws, whether on the slope or on the plane; the position and size of the *in-situ* machined QR code patterns are consistent with the design in the software.

3.3.3. Case 3: Machining on a curved surface with different pixel distance

In order to verify the machining capacity on a curved surface, an aluminum alloy arc surface workpiece (40 mm × 40 mm × 11.5 mm) was selected as the processing object, and the pattern was projected after equal arc length transformation. The machining line spacing was artificially adjusted by the pixel distance in the *in-situ* machining software. The measurement and projection results are presented in Fig. 9(a). A machining line spacing of 40 and 120 μm was used, respectively. The machining results are shown in Figs. 9(b) and (c). When the machining line spacing was 40 μm, the machined pattern was filled (Fig. 9(b)); when it was changed to 120 μm, there was a gap between each machining line (Fig. 9(c)). Optical microscopy observation in the range of the red dotted box (Fig. 9) showed that the line width produced by the laser was (46.08 ± 1.22) μm, and the actual machining line spacing was (40.04 ± 0.72) and (120.11 ± 0.02) μm, respectively, which is consistent with the design values; this indicates that the system has high processing accuracy.

3.3.4. Case 4: Tool in-situ measurement and micro-textures processing

Cutting tools with micro-textures can reduce friction and improve wear resistance and anti-adhesion. The proposed methods can achieve the online and *in-situ* measurement of a tool and fabricate micro-textures without the fixture. Fig. 10(a) shows a triangular turning tool with a particular rake angle. The scanned laser line spacing is 0.2 mm. The reconstruction results (Fig. 10(b)) clearly show the rake face and rake angle of the tool. The measured tool profile was extracted (Fig. 10(c)) and the length of the three sides and the diameter of the hole were measured using DigitalMicrograph software. When considering the tool nose radius, the actual side length L_r was $L_r = L_i - 2 \times \left(\sqrt{3} - 1\right)R$, where R is the tool nose radius, which is 0.2 mm, and L_i is the side length without considering R, as shown in Fig. 10(c). The *in-situ* measured value considering the R and the Vernier caliper measured value are listed in Table 1. The measurement absolute error of thickness was 3 μm, and the absolute errors of the side length and hole diameter (D) were within 90 μm. The micro-textures were imported by *in-situ* machining software and projected on the rake face (Fig. 10(d)). The machining results of the micro-textures are shown in Fig. 10(e), and reflect an accurate processing position and uniform grooves. This method can satisfy the requirements for

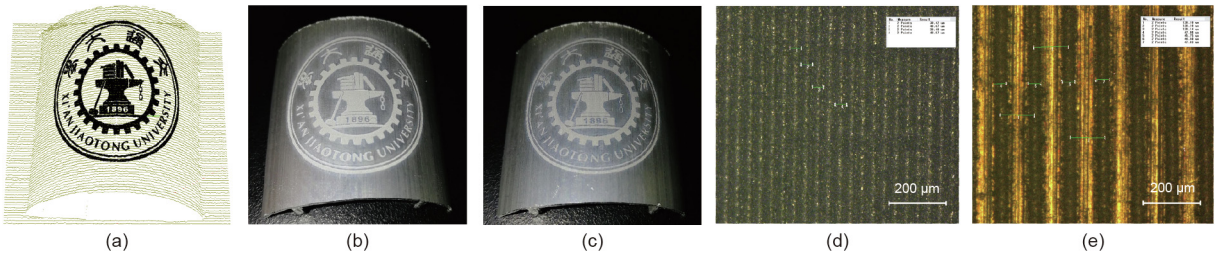

Fig. 9. Implementation process and results of Case 3. (a) Measurement and projection results of the aluminum alloy arc surface workpiece. *In-situ* machining results with (b) 40 μm machining line spacing and (c) 120 μm machining line spacing. Optical microscopy observation results with (d) 40 μm machining line spacing and (e) 120 μm machining line spacing.

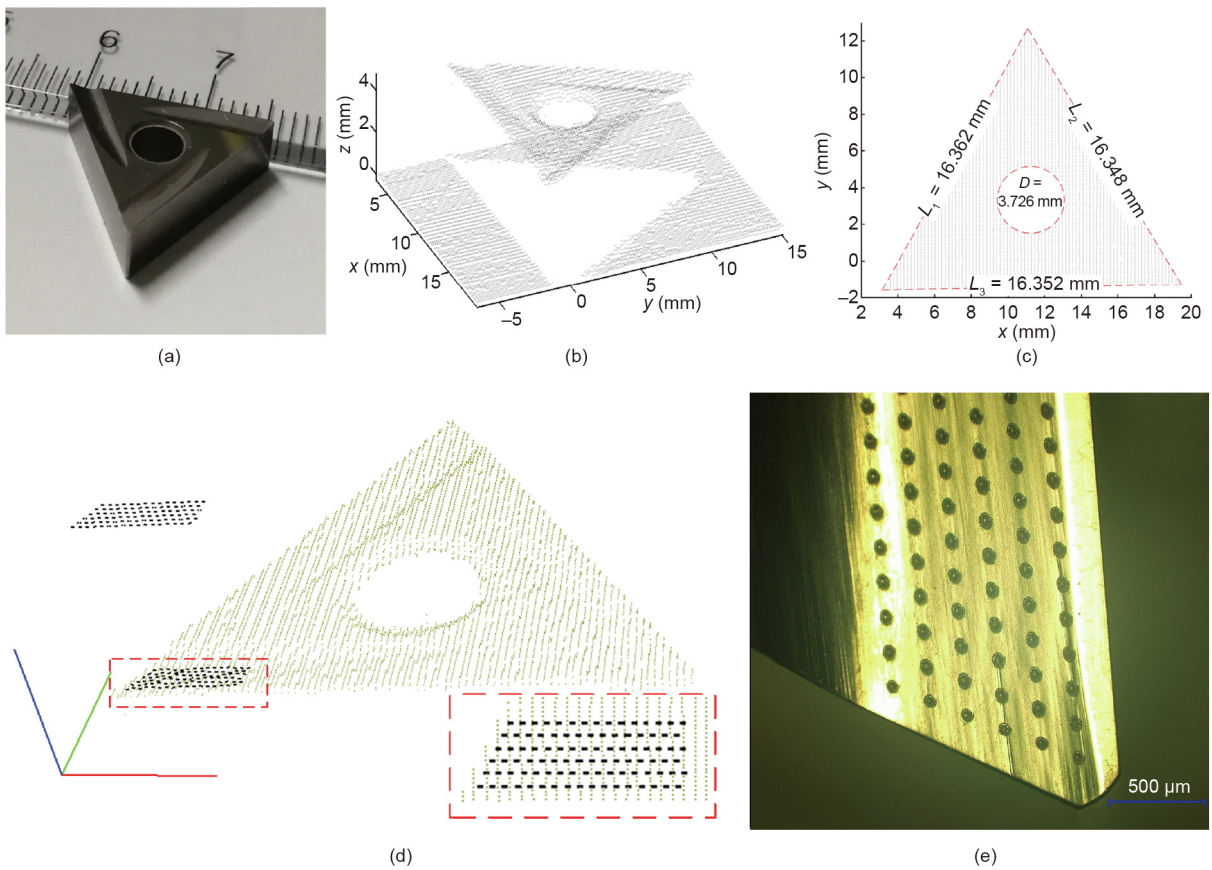

Fig. 10. Implementation process and results of Case 4. (a) Triangular turning tool with a particular rake angle; (b) reconstruction results of the tool; (c) top view of the tool profile (the dimensions in the figure are measured by DigitalMicrograph software); (d) *in-situ* machining software screenshot (bottom right corner is the top view of the projection of the micro-textures); (e) *in-situ* machining results of the micro-textures. L_1, L_2, L_3: the side length without considering the tool nose radius.

Table 1
The *in-situ* measured value and the Vernier caliper measured value of the tool.

Dimension	*In-situ* measured value (mm)	Vernier caliper measured value (mm)	Absolute error (mm)	Relative error (%)
Thickness	4.683	4.68	0.003	0.06
L_1	16.069	16.14	−0.071	0.44
L_2	16.055	16.14	−0.085	0.53
L_3	16.059	16.14	−0.081	0.50
D	3.726	3.80	−0.074	1.95

D: hole diameter.

manufacturing different tool micro-textures by optimizing the micro-texture design and the laser processing parameters; thus, this case reflects the practical application value of the *in-situ* laser machining system.

4. Discussion

Unlike the conventional line structured light measurement method, in which the laser line is directly generated by the line

laser, the laser line in this study was generated by a galvanometer scanner. Because the position of the laser line in the common method cannot be accurately controlled, it is necessary to calibrate the light plane to obtain the light plane equation; a great deal of research has been conducted on this topic. For example, Liu et al. [40] used a ball target and nonlinear optimization to perform the light plane calibration, while Kiddee et al. [41] projected cross-line structured light (CLSL) on the chessboard to calculate the light plane equation. These calibration methods are complicated and require accurate calibration targets. In this study, the position of the laser line can be precisely controlled by the galvanometer scanner, thus eliminating the need for light plane calibration, which greatly simplifies the process and reduces the workload. 3D reconstruction by means of the typical line structured light measurement method requires additional linear or rotary motion axes to achieve laser line scanning of the workpiece. However, the galvanometer scanner can realize self-scanning, thereby eliminating the need to add additional motion axes, and consequently saving hardware cost. Therefore, line structured light measurement method using a galvanometer scanner has technical and cost advantages.

Compared with a 2D galvanometer scanner, a 3D galvanometer scanner must acquire the 3D information of the workpiece in order to accurately focus the laser. However, most laser machining systems equipped with a 3D galvanometer scanner lack the 3D measurement capability, making it necessary to obtain the 3D information of the workpiece through other methods or equipment in advance; this is inconvenient and will increase the time cost and workload. The proposed methods add 3D measurement capability to the 3D laser machining system with just one industrial camera. The typical 3D laser machining process mainly includes 3D modeling, importing the models, and positioning the workpieces by the fixture. In comparison, the proposed methods do not require fixture positioning. *In-situ* measurement can obtain the 3D information of the workpiece and match the machining coordinate system, so that the laser can be focused on a certain position of the workpiece. The above method realizes a simple operation process for laser 3D machining, which greatly reduces time and labor costs.

When the workpiece size is large, the farther away a point on the workpiece surface is from the origin of the world coordinate system, the more obvious the measurement error will be. This error is due to inaccurate calibration of the camera parameters. If the measured height is inaccurate, the laser focus will be defocused during the 3D laser processing, which will directly affect the processing quality. In order to ensure measurement accuracy in the height direction, the height calibration method was proposed. This method ensures that the height error is always within a certain range, which is generally smaller than the laser Rayleigh length in the laser machining system, thereby ensuring that the laser is always focused. The error of the height calibration method mainly comes from the line structured light not being thin enough and the resolution of the camera not being high; however, the error is stable and within an acceptable range.

5. Conclusion

In this study, an a 3D *in-situ* laser machining system integrating laser measurement and machining was built by using a 3D galvanometer scanner equipped with a side-axis industrial camera. The line structured light was projected onto the workpiece surface by the galvanometer scanner, which increased the 3D measurement capability for the 3D laser machining system. A line structured light measurement model based on the galvanometer scanner was proposed. A method using camera parameters and the light plane equation was used to obtain the 3D surface information. A height calibration method was proposed to further ensure the measurement accuracy. The measurement error of these methods is stable and acceptable in the height direction. The feasibility and practicability of this *in-situ* laser machining system were verified using specific cases.

The advantages of the proposed methods are as follows: ① Compared with the conventional line structured light measurement method, the proposed methods do not require light plane calibration and additional motion axes to achieve 3D reconstruction, and thus provide technical and cost advantages; ② the *in-situ* laser machining system realizes a simple operation process by the integration of 3D *in-situ* measurement and laser machining, which greatly reduces labor and time costs.

For tasks that require high machining accuracy, the *in-situ* laser machining system can realize higher precision laser processing on a macro–micro scale by configuring a more precise coaxial vision device (such as SCANLAB's camera adapter), which has great research value and application potential.

Acknowledgements

This work was supported by the National Key Research and Development Program of China (2017YFB1104602 and 2016YFB1102502) and the Program for Changjiang Scholars and Innovative Research Team in University (IRT_15R54).

Compliance with ethics guidelines

Xiao Li, Bin Liu, Xuesong Mei, Wenjun Wang, Xiaodong Wang, and Xun Li declare that they have no conflict of interest or financial conflicts to disclose.

References

[1] Yang L, Cui J, Wang Y, Hou C, Xie H, Mei X, et al. Nanospot welding of carbon nanotubes using near-field enhancement effect of AFM probe irradiated by optical fiber probe laser. RSC Adv 2015;5(70):56677–85.
[2] Cui J, Yang L, Wang Y. Nanowelding configuration between carbon nanotubes in axial direction. Appl Surf Sci 2013;264(1):713–7.
[3] Cui J, Zhang J, He X, Yang X, Mei X, Wang W, et al. Atomistic simulations on the axial nanowelding configuration and contact behavior between Ag nanowire and single-walled carbon nanotubes. J Nanopart Res 2017;19(3):90.
[4] Dubey AK, Yadava V. Laser beam machining—a review. Int J Mach Tools Manuf 2008;48(6):609–28.
[5] Gao S, Huang H. Recent advances in micro- and nano-machining technologies. Front Mech Eng 2017;12(1):18–32.
[6] Duan W, Wang K, Dong X, Mei X, Wang W, Fan Z. Experimental characterizations of burr deposition in Nd:YAG laser drilling: a parametric study. Int J Adv Manuf Technol 2015;76(9–12):1529–42.
[7] Fan Z, Dong X, Wang K, Duan W, Wang R, Mei X, et al. Effect of drilling allowance on TBC delamination, spatter and re-melted cracks characteristics in laser drilling of TBC coated superalloys. Int J Mach Tools Manuf 2016;106:1–10.
[8] Hong KM, Shin YC. Prospects of laser welding technology in the automotive industry: a review. J Mater Process Technol 2017;245:46–69.
[9] Sun X, Wang W, Mei X, Pan A, Liu B, Li M. Controllable dot-matrix marking on titanium alloy with anti-reflective micro-structures using defocused femtosecond laser. Opt Laser Technol 2019;115:298–305.
[10] Wang X, Zheng H, Wan Y, Feng W, Lam YC. Picosecond laser surface texturing of a Stavax steel substrate for wettability control. Engineering 2018;4(6):816–21.
[11] Pan A, Wang W, Liu B, Mei X, Yang H, Zhao W. Formation of high-spatial-frequency periodic surface structures on indium-tin-oxide films using picosecond laser pulses. Mater Des 2017;121:126–35.
[12] Li J, Wang W, Mei X, Sun X, Pan A. The formation of convex microstructures by laser irradiation of dual-layer polymethylmethacrylate (PMMA). Opt Laser Technol 2018;106:461–8.
[13] Shao J, Ding Y, Wang W, Mei X, Zhai H, Tian H, et al. Generation of fully-covering hierarchical micro-/nano-structures by nanoimprinting and modified laser swelling. Small 2014;10(13):2595–601.
[14] Yoo HW, Ito S, Schitter G. High speed laser scanning microscopy by iterative learning control of a galvanometer scanner. Control Eng Pract 2016;50:12–21.
[15] Luo X, Li J, Lucas M. Galvanometer scanning technology for laser additive manufacturing. In: Gu B, Helvajian H, Piqué A, Dunsky CM, Liu J, editors. SPIE:

Proceedings of the SPIE 10095, Laser 3D manufacturing IV; 2017 Jan 28–Feb 2; San Francisco, CA, USA. Bellingham: SPIE.
[16] Yu Y, Bai S, Wang S, Hu A. Ultra-short pulsed laser manufacturing and surface processing of microdevices. Engineering 2018;4(6):779–86.
[17] Cao BX, Hoang PL, Ahn S, Kim J, Noh J. High-precision detection of focal position on a curved surface for laser processing. Precis Eng 2017;50:204–10.
[18] Noh J, Cho I, Lee S, Na S, Lee JH. Fabrication of microgrooves on a curved surface by the confocal measurement system using pulse laser and continuous laser. Rev Sci Instrum 2012;83(3):033106.
[19] Noh J, Suh J, Na S. Fabrication of microgrooves on roll surfaces using a scanner and a telecentric lens. Jpn J Appl Phys 2010;49(5):311–33.
[20] Cao BX, Bae M, Sohn H, Choi J, Kim Y, Kim JO, et al. Design and performance of a focus-detection system for use in laser micromachining. Micromachines (Basel) 2016;7(1):E2.
[21] Wang X, Duan J, Jiang M, Ke S, Wu B, Zeng X. Study of laser precision ablating texture patterns on large-scale freeform surface. Int J Adv Manuf Technol 2017;92(9–12):4571–81.
[22] Yan H, Chen J, Shao J. Study on laser dots marking based on dynamic focusing galvanometer system. Chin J Lasers 2013;40(9):91–6.
[23] Liu H, Wang S, Ma C, Wang H. Study on an actuator with giant magnetostrictive materials for driving galvanometer in selective laser sintering precisely. Int J Mechatronics Manuf Syst 2015;8(3–4):116–33.
[24] Xiao HB, Zhou YQ, Liu MJ. Experimental research on 3D ultraviolet laser precision marking processing technology. In: Proceedings of the 2nd International Conference on Computer, Mechatronics and Electronic Engineering; 2017 Dec 24–25; Xiamen, China. Lancaster: DEStech Publications, Inc.; 2017. p. 516–20.
[25] Diaci J, Bračun D, Gorkič A, Možina J. Rapid and flexible laser marking and engraving of tilted and curved surfaces. Opt Lasers Eng 2011;49(2):195–9.
[26] Li X, Lian Q, Li D, Xin H, Jia S. Development of a robotic arm based hydrogel additive manufacturing system for *in-situ* printing. Appl Sci 2017;7(1):73.
[27] Lian Q, Li X, Li D, Gu H, Bian W, He X. Path planning method based on discontinuous grid partition algorithm of point cloud for *in situ* printing. Rapid Prototyping J 2019;25(3):602–13.
[28] Everton SK, Hirsch M, Stravroulakis P, Leach RK, Clare AT. Review of *in-situ* process monitoring and *in-situ* metrology for metal additive manufacturing. Mater Des 2016;95:431–45.
[29] Goda I, L'Hostis G, Guerlain P. *In-situ* non-contact 3D optical deformation measurement of large capacity composite tank based on close-range photogrammetry. Opt Lasers Eng 2019;119:37–55.
[30] Geng J. Structured-light 3D surface imaging: a tutorial. Adv Opt Photonics 2011;3(2):128–60.
[31] Salvi J, Fernandez S, Pribanic T, Llado X. A state of the art in structured light patterns for surface profilometry. Pattern Recognit 2010;43(8):2666–80.
[32] Zhang S. High-speed 3D shape measurement with structured light methods: a review. Opt Lasers Eng 2018;106:119–31.
[33] Perhavec T, Gorkič A, Bračun D, Diaci J. A method for rapid measurement of laser ablation rate of hard dental tissue. Opt Laser Technol 2009;41(4):397–402.
[34] Zhou P, Xu K, Wang D. Rail profile measurement based on line-structured light vision. IEEE Access 2018;6:16423–31.
[35] Liu S, Tan Q, Zhang Y. Shaft diameter measurement using structured light vision. Sensors (Basel) 2015;15(8):19750–67.
[36] Li J, Liu G, Liu Y. A dynamic volume measurement system with structured light vision. In: Proceedings of 2016 31st Youth Academic Annual Conference of Chinese Association of Automation; 2016 Nov 11–13; Wuhan, China. New York: IEEE; 2016. p. 251–5.
[37] Goshtasby A, Shyu HL. Edge detection by curve fitting. Image Vis Comput 1995;13(3):169–77.
[38] Steger C. An unbiased detector of curvilinear structures. IEEE Trans Pattern Anal Mach Intell 1998;20(2):113–25.
[39] Xie Z, Wang X, Chi S. Simultaneous calibration of the intrinsic and extrinsic parameters of structured-light sensors. Opt Lasers Eng 2014;58:9–18.
[40] Liu Z, Li X, Li F, Zhang G. Calibration method for line-structured light vision sensor based on a single ball target. Opt Lasers Eng 2015;69:20–8.
[41] Kiddee P, Fang Z, Tan M. A practical and intuitive calibration technique for cross-line structured light. Optik 2016;127(20):9582–602.